Monthly Notices of the ROYAL ASTRONOMICAL SOCIETY LETTERS

Mon. Not. R. Astron. Soc. **407,** L59–L63 (2010) doi:10.1111/j.1745-3933.2010.00904.x

Broad and luminous [O III] and [N II] in globular cluster ULXs

R. L. Porter★

Department of Astronomy, University of Michigan, 500 Church Street, Ann Arbor, MI 48109-1042, USA

Accepted 2010 June 12. Received 2010 June 11; in original form 2010 May 19

ABSTRACT

We consider an accretion disc origin for the broad and luminous forbidden line emission observed in ultraluminous X-ray (ULX) sources CXOJ033831.8−352604 and XMMU 122939.7+075333 in globular clusters hosted by elliptical galaxies NGC 1399 and 4472, respectively. We will refer to the latter by the globular cluster name RZ2109. The first has strong [O III] and [N II], the second only [O III]. Both Hα and Hβ are very weak or undetected in both objects. We assume that the large linewidths are due to Keplerian rotation around a compact object and derive expressions for maximum line luminosities. These idealized models require central masses $\gtrsim$100 and $\gtrsim$30 000 $M_\odot$ for CXOJ033831.8−352604 and RZ2109, respectively. An independent, bootstrap argument for the total disc mass yields, for both systems, $M_{\rm disc} \gtrsim 10^{-4}\,M_\odot$ for a purely metallic disc (and two orders of magnitude larger for solar metallicities). If Roche lobe overflow is implicated, viscous time-scales are $\gtrsim$300 yr. Standard disc theory then offers another limit on the central masses. Lobe radii for an $\sim$1 $M_\odot$ donor are $\gtrsim 10^{13}$ cm. We therefore rule out Roche lobe overflow of a white dwarf in both systems. Red giants could fill the necessary lobes. Whether they are too metal poor to produce the strong forbidden lines without strong hydrogen emission is unclear.

Key words: accretion, accretion discs – galaxies: individual: NGC 1399 – galaxies: individual: NGC 4472 – galaxies: star clusters: general.

1 INTRODUCTION

Ultraluminous X-ray (ULX) sources are point sources that appear to exceed the Eddington luminosities of stellar mass compact objects. They are therefore prime candidates for long-sought intermediate-mass black holes (IMBHs). ULXs have been studied extensively since their discovery in the early 1980s, and they continue to be the subjects of intense research activity (Miller, Fabian & Miller 2004; Winter, Mushotzky & Reynolds 2006; Hui & Krolik 2008; King 2008, 2009).

Zepf et al. (2007, 2008, hereafter Z08) and Irwin et al. (2010, hereafter I10) recently identified very broad and luminous [O III] λ5007 emission in two ULXs harboured by globular clusters in elliptical galaxies NGC 4472 and 1399, respectively. The connections to globular clusters are robust, as in both I10 and Z08; we see large redshifts that agree very well with the redshifts of the clusters and their host galaxies. Linewidths were 140 and 1500 km s^{-1} in the two systems, and line luminosities, assuming the sources radiate isotropically, were 10^{36}–10^{37} erg s^{-1}. Both Z08 and I10 found difficulty simultaneously explaining the linewidths and luminosities with an accretion disc around a stellar black hole, the most natural explanation for a consistent source with $L_{\rm x} \approx 10^{39}$ erg s^{-1}. The observed lines created a tension. Their large linewidths suggested rapid rotation very close to the source, while the large luminosities suggested a large line-emitting region and an origin in the outer disc. The lack of Hα and Hβ presented further complications in the context of globular clusters. Z08 suggested that a stellar black hole wind is the explanation for RZ2109. I10 suggested for CXOJ033831.8−352604 tidal disruption of a white dwarf by an IMBH (Fabian, Pringle & Rees 1975; Rosswog, Ramirez-Ruiz & Hix 2009).

This Letter is organized as follows. In Section 2, we revisit and extend the arguments presented by Z08 and I10, first relaxing the assumption that the line-emitting gas cannot be denser than the critical density of the observed lines. We derive a simple expression for the maximum line luminosity in an accretion disc geometry. Our expression is independent of temperature, density and metallicity, and depends only on rotational velocity and central mass. While a supercritical density alleviates some of the tension described above, we none the less confirm the Z08 and I10 conclusions that stellar mass accretion cannot be implicated in either ULX. In Section 3, we present bootstrap arguments for the total mass in an accretion disc and obtain lower limits. In Section 4, we explore the implications for Roche lobe overflow.

2 MAXIMUM LINE LUMINOSITIES

Here we derive expressions for the maximum line luminosities of the [O III] and [N II] forbidden lines. We focus on the [O III] lines because they are seen in both objects. Because both [N II] and [O III]

★E-mail: rlporter@umich.edu

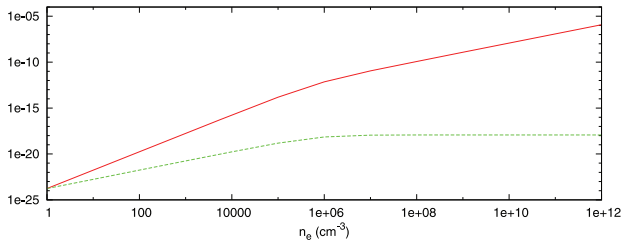

Figure 1. [O III] λ5007 emissivity (red solid line, erg cm^{-3} s^{-1}) and intensity (green dashed line, erg cm^{-2} s^{-1}) emitted in an isothermal, constant-density line of sight with solar metallicity and column density 1 cm^{-2}. Each curve is a function of volume density. The critical density can be seen as a 'knee' in each curve near $n_e = 10^6$ cm^{-3}.

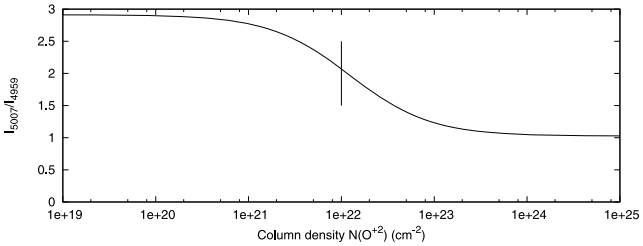

Figure 2. Theoretical ratio of the lines in the [O III] doublet λλ 4959, 5007 as a function of O^{+2} column density. Observations in both Z08 and I10 clearly suggest ratios towards the canonical optically thin value. The vertical bar marks $N(O^{+2}) = 10^{22}$ cm^{-2} (or $\tau_{5007} = 1$).

are produced by ions of the carbon isoelectronic sequence, our formalism applies to both. The final expression is independent of temperature, density and metallicity and depends only on rotational velocity and central mass.

We assume the gas is photoionized and collisionally excited and begin by writing a simple two-level balance equation:

$$n_e n_1 q_{12} = n_e n_2 q_{21} + n_2 A_{21}, \tag{1}$$

where n_1 and n_2 are the populations of the lower and upper levels, A_{21} is the spontaneous radiative transition probability (s^{-1}) from level 2 to level 1 and q_{12} and q_{21} are the collisional excitation and de-excitation coefficients (cm^3 s^{-1}) and are related by $q_{12} = (\omega_2/\omega_1)\, q_{21} \exp(-h\nu/kT)$. The critical density $n_{\rm crit} \equiv A_{21}/q_{21}$ is the density at which the collisional de-excitation rate ($n_e q_{21}$) equals the radiative decay rate. For $n_e \ll n_{\rm crit}$, the radiative decay dominates and the population of level 2 is

$$n_2 = \frac{n_e n_1 q_{12}}{A_{21}}. \tag{2}$$

For $n_e \gg n_{\rm crit}$, the usual Boltzmann equation of local thermodynamic equilibrium (LTE) applies. The local emissivity is $\epsilon = n_2 h\nu_{21} A_{21}$, and it follows that

$$\epsilon = \begin{cases} n_e n_1 q_{12} h\nu_{21} & n_e \ll n_{\rm crit}, \\ n_1 \frac{\omega_2}{\omega_1} \exp(-h\nu/kT) h\nu_{21} A_{21} & n_e \gg n_{\rm crit}. \end{cases} \tag{3}$$

The critical density marks the transition from the regime where radiative cooling is proportional to $n_e\, n_{\rm ion}$ to the LTE regime where cooling is proportional to $n_{\rm ion}$. The emitted energy per unit volume per unit time increases monotonically with increasing density. The two regimes are illustrated in Fig. 1 for the [O III] λ5007 line. The critical density is represented by the knee near 10^6 cm^{-3}.

Both I10 and Z08 considered the low-density case, and we have no need to reconsider that here. The remainder of this Letter will assume $n_e > n_{\rm crit}$. Authors who have discussed the high-density behaviour of [O III] emission include Nussbaumer & Storey (1981), Keenan & Aggarwal (1987), Kastner & Bhatia (1989) and Osterbrock & Ferland (2006). From an observational perspective, we note, for example, Andreä, Drechsel & Starrfield (1994) found n_e as high as 10^8 cm^{-3} from [O III] lines in classical novae.

We generalize the high-density emissivity to multilevel configurations by using the O^{+2} calculations of Nussbaumer & Storey (1981). Their calculations are valid for all practical densities and include temperatures as high 40 000 K, safely above the temperature of photoionized O^{+2} gas considered in Section 3. The upper level of the [O III] λ5007 and [N II] λ6548 transitions is $^1D_2$. The fractional population $f(^1D_2)$ in table 5 of Nussbaumer & Storey does not exceed ≈0.2. A comparable value applies to N^+, and our emissivities take the maximum value

$$\epsilon_{\rm max} = n_A f(^1D_2)_{\rm max} h\nu_{21} A_{21}, \tag{4}$$

where n_A is the density of the ionization stage.

Next we posit a column of gas having local emissivity given by equation (4). The intensity emitted through the column is

$$I_\lambda = \int \epsilon \mathrm{d}z, \tag{5}$$

where z represents position along the column (or above an annulus perpendicular to the plane of the accretion disc). To impose an upper limit on the integration variable, we introduce a photon escape probability, $P_{\rm esc} = 1/(1+\tau)$, where τ is the (Napier) line-centre optical depth. Equation (5) is then written as

$$I_\lambda^{\rm max} = N_A f(^1D_2)_{\rm max} h\nu_{21} A_{21} P_{\rm esc}, \tag{6}$$

where we have used $N_A = n_A \int \mathrm{d}z$.

Equation (6) saturates at $\tau \approx 1$, consistent with the rule of thumb that we can see into a cloud only up to optical depth unity (e.g. Rybicki & Lightman 1979). The upper limit corresponds to $N(O^{+2}) \approx 10^{22}$ cm^{-2}, assuming local linewidths are thermal at ≈10^4 K. Optical depth in the [O III] lines causes their relative strengths to decrease from the canonical 3:1 ratio to approximate parity in the optically thick limit. This behaviour is shown in Fig. 2. The plotted ratio is visibly greater than unity in both Z08 and I10. Our limit, therefore, has the consequence of preventing model line ratios inconsistent with the observations.

Note that equation (6) does not depend upon density. The green dashed curve in Fig. 1 illustrates this and is an important point in our analysis. Above the critical density, the intensity emitted through a fixed column density is independent of the volume density of the gas. This means that, with no penalty on the total intensity, we can increase the density and, with all else fixed, squeeze the gas into a smaller volume, potentially allowing a stellar mass black hole explanation.

Finally, we obtain a maximum luminosity via an effective surface area. We define the inner radius, r_0, of our line-emitting region by assuming the line-emitting gas is in a Keplerian orbit about central mass M with velocity v (which we relate to observed linewidths below) so that

$$r_0 = GM/v^2. \tag{7}$$

We assume the line-emitting region comprises an annulus with width comparable to r_0. Line luminosities are written as

$$L_\lambda = 4\pi r_0^2 I_\lambda = 4\pi \left(\frac{GM}{v^2}\right)^2 I_\lambda. \tag{8}$$

We evaluate constants, normalize variables to convenient values and obtain maximum luminosity

$$L_\lambda^{\rm max} = L_\lambda^0 {M_1}^2 {v_{100}}^{-4}, \tag{9}$$

Table 1. Observed and model luminosities (erg s^{-1}). The last column contains the L_λ^0 values defined via equation (9).

Quantity	CXOJ033831.8−352604	RZ2109	L_λ^0
L_{5007}	Few $\times 10^{36}$	1.4×10^{37}	2.4×10^{33}
L_{6584}	3×10^{36}	Unobs.	2.8×10^{32}
$L_{\rm x}$	1.5–2.3 $\times 10^{39}$	4×10^{39}	

where M_1 is the central mass in units $M_\odot$, v_{100} is the rotational velocity in units 100 km s^{-1} and all constants have been absorbed into fiducial values L_λ^0. Table 1 contains the fiducial luminosities for [O III] λ5007 and [N II] λ6584. Atomic data used in this section are from Wiese, Fuhr & Deters (1996), as obtained from the NIST Atomic Spectra Database (Ralchenko et al. 2008).

It is important to emphasize that equations (8) and (9) are independent of temperature, volume density and metallicity. This is by design. However, temperature and metallicity do inform the *practicality* of the equations. We will discuss the former below. Regarding the latter, at fixed $n_{\rm e}$, the disc height required to reach a certain column density (and therefore luminosity) is inversely proportional to metallicity. A purely metallic plasma allows the smallest disc height for the maximum-luminosity configuration of our model. Solar metallicity gas requires a disc height more than three orders of magnitude greater, reaching ≈10 Thomson depths. Scattering would yield emergent linewidths ∼1000 km s^{-1}. Such large widths would contradict our rotational broadening assumption in both ULXs and are ruled out completely by observation in CXOJ033831.8−352604. If the width scales as the number of scatterings (usually the greater of τ and τ^2), this problem would be eliminated by decreasing the column by some factor. The minimum central mass found below would increase by the square of that factor.

We plot in Fig. 3 maximum line luminosities as a function of the velocity of the gas at r_0. Several values of the compact object mass are considered. The middle two lines represent recent theoretical (80 $M_\odot$) and observed (30 $M_\odot$) upper limits to the mass of a stellar black hole (Belczynski et al. 2010). Results for I10 and Z08 are indicated by the squares, where we have assumed velocities equal to $1/(2\sqrt{\ln 2})$ times the measured FWHM. This ignores the

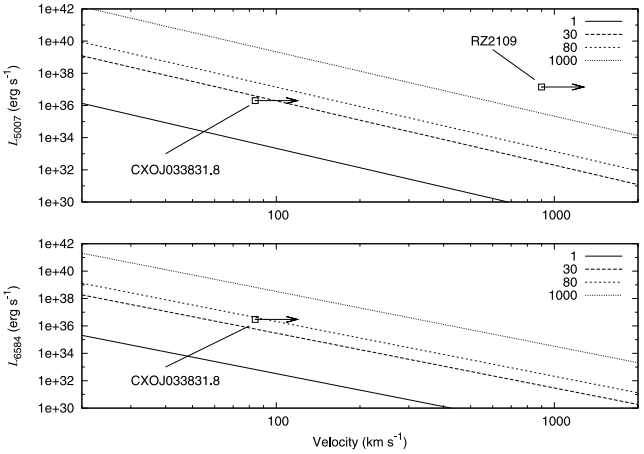

Figure 3. Maximum line luminosities (upper panel: [O III] λ5007; lower panel: [N II] λ6584) versus rotational velocity of the line-emitting region for several values of the central mass (in units $M_\odot$). Squares indicate results from I10 and Z08. Arrows point from minimum (edge-on) velocity to the velocity appropriate for 45° inclination. [N II] was not detected in RZ2109.

effect of disc inclination on the observed linewidths. Accounting for inclination would mean a greater rotational velocity and a smaller annulus radius (for a given central mass). This would decrease the surface area of the line-emitting region and the luminosity of the line. The arrow on each square points to the velocity appropriate for the (arbitrarily chosen) inclination angle of 45°.

The point corresponding to CXOJ033831.8−352604 in the upper panel of Fig. 3 is beneath the lines corresponding to the theoretical and observed stellar mass black hole upper limits. However, the lower panel of Fig. 3 makes a more compelling case. The observed L_{6584} is very slightly less than (at edge-on inclination) the maximum predicted luminosity corresponding to the maximum theoretical mass of a stellar black hole (Belczynski et al. 2010). Note that these predictions assume optimal cooling efficiency. I10 found $T_{\rm e} \leq 13\,000$ K in the [N II] emitting region using the lack of λ5755. Using this temperature would lower the [N II] predictions by a factor of ∼2 and require $M \gtrsim 100\,M_\odot$. [O III] λ4363 was neither presented nor mentioned in I10. Measurement of this line could place a strong constraint on the temperature of the [O III] region.

The upper panel of Fig. 3 clearly demonstrates that the Z08 observations of RZ2109 cannot be explained as Keplerian rotation around a stellar mass object. The required mass is at least 6000 $M_\odot$. [O III] λ4363 is weakly detected in RZ2109. A rough estimate is that λ5007 is at least 10 times greater. The Nussbaumer & Storey (1981) tabulations would then give $T \lesssim 15\,000$ K at the λ5007 critical density. That upper limit quickly decreases to $T \lesssim 7500$ K for $n_{\rm e} \gtrsim 10^7$ cm^{-3}. These considerations depress the maximum luminosity by at least a factor of 20, so that the minimum central mass is at least 30 000 $M_\odot$.

We rule out stellar black hole Keplerian accretors in both sources. Sub-Keplerian motions have orbiting radii that are smaller for a given central mass than Keplerian, decreasing the surface area of the line-emitting region and exacerbating the problems discussed above. We can therefore rule out sub-Keplerian, stellar black hole accretion more readily than we can rule out Keplerian.

We stress that the two panels of Fig. 3 do not depend upon the relative abundances of oxygen and nitrogen. The predicted [N II] luminosities are noticeably less than the [O III] luminosities at the same velocity and central mass. This is because the [N II] lines are less efficient coolants than their [O III] counterparts.

3 TOTAL DISC MASS

Here we present a bootstrap argument for the total disc masses in an accretion scenario. The mass required to emit L_{5007} (or L_{6584}) is

$$M(^1D_2) = \frac{Zm_p L_\lambda}{h\nu A}, \tag{10}$$

where Zm_p is the mass of a single atom with mass number Z. This is independent of the geometrical model and the gas density (even below $n_{\rm crit}$), and accounts only for the population in the upper level of the transition. Observed values of L_λ are listed in Table 1. The [O III] lines require masses $\sim 3 \times 10^{-7}$ and $\sim 2 \times 10^{-6}\,M_\odot$ for CXOJ033831.8−352604 and RZ2109, respectively. The [N II] lines in CXOJ033831.8−352604 require $4 \times 10^{-6}\,M_\odot$.

We can bootstrap our way to a total disc mass via

$$\frac{M(^1D_2)}{M_{\rm disc}} = \frac{\rho_Z}{\rho} \frac{\int f_{\rm ion} f(^1D_2) r\,{\rm d}r}{\int r\,{\rm d}r}, \tag{11}$$

where $f(^1D_2)$ was discussed in Section 2 and $f_{\rm ion}$ is the C-like ionization fraction, which we estimate using the well-known plasma simulation code CLOUDY (version C08, last described by Ferland

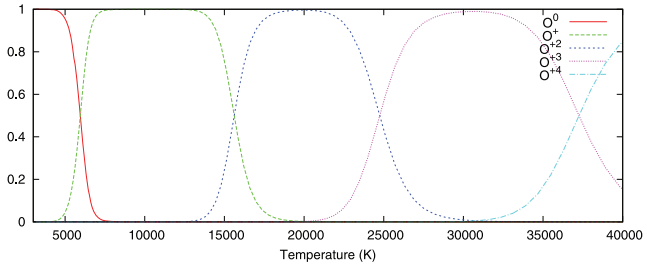

Figure 4. Ionization fractions of oxygen as a function of the temperature of an intense blackbody.

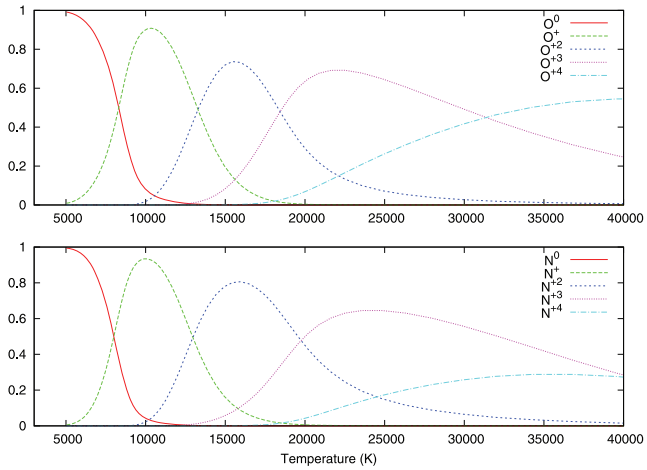

Figure 5. Ionization fractions of oxygen (upper panel) and nitrogen (lower panel) as a function of the electron temperature of gas ionized by a power-law continuum with spectral index $\Gamma = 2.5$.

et al. 1998). Fig. 4 plots the results for oxygen as a function of the temperature of a bright blackbody photoionization source. The fraction in O^{+2} peaks around 20 000 K. The maximum equivalent width of λ5007 with $N(O^{+2}) = 10^{22}$ cm^{-2} against a blackbody of the same area and $T_{BB} = 20\,000$ K is about 1 Å. We estimate from spectra in I10 and Z08 observed equivalent widths of 5 and 15 Å. Blackbody sources with weak enough continuum at ∼5000 Å are too weak to ionize O^{+}. We require a harder continuum.

We instead consider, again using CLOUDY, a power-law continuum with spectral index $\Gamma = 2.5$ (following X-ray continuum fits in I10). Fig. 5 plots both oxygen and nitrogen ionization fractions as a function of electron temperature. The ionization parameter ranges from $-9 \leq \log U \leq 0$.

The fractions $f_{\rm ion}$ and $f(^1D_2)$ depend on temperature. We relate them to the variable of integration r via the standard Shakura & Sunyaev (1973) prescription ($T \propto r^{-3/4}$). The ratio of integrals in equation (11) is illustrated by the dotted blue curves in Fig. 6. The result depends on the upper limit of integration. The peak is ≈4 per cent for both oxygen and nitrogen. The curves decline as r^{-2} at large radii.

An important conclusion can be derived from Figs 5 and 6. The regions emitting [O III] and [N II] are mostly non-cospatial. The details depend on the ionizing source and the geometry. Since the second ionization energy of nitrogen is only 85 per cent of the second ionization energy of oxygen, the basic result is fairly robust. N^{+} always peaks at a temperature significantly less than the temperature of the O^{+2} peak. If the standard α-disc is applicable, we have $T \propto r^{-3/4}$. Keplerian rotation gives $v \propto r^{-1/2}$, so $v \propto T^{2/3}$. A series of tests suggests the [O III] and [N II] linewidths should differ by a

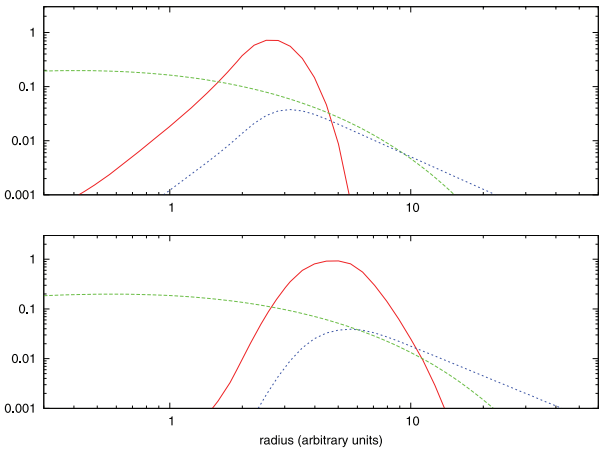

Figure 6. Level and ionization stage fractions of oxygen (upper panel) and nitrogen (lower panel) versus normalized radius. Solid red lines are fractions in O^{+2} and N^{+}, dashed green lines are $f(^1D_2)$ and dotted blue lines are ratios of integrals given in the right-hand side of equation (11).

factor of $\gtrsim$1.4. The widths are uncertain but appear comparable in the I10 observations. This argues against Keplerian rotation about *any* central mass in CXOJ033831.8−352604. A very steep temperature gradient or a thermal instability between the [O III] and [N II] regions could mitigate this problem. High-resolution spectroscopy would be useful in efforts to address such questions.

Finally, we require the density of oxygen relative to the total gas density. Assuming metallicity is independent of radius, we can write

$$\frac{\rho_Z}{\rho} = \frac{A\, n_Z}{\Sigma\, A\, n_Z}, \tag{12}$$

where A is atomic mass number. For fixed relative metal abundances, the fraction of mass in oxygen varies from ∼0.005 with solar abundances (Grevesse & Sauval 1998) to ∼0.4 for all metals.

Combining the above results, we find $M_{\rm disc} \gtrsim 10^{-4}\,{\rm M}_\odot$. This corresponds to the purely metallic case. If we assume roughly solar abundances, $M_{\rm disc} \gtrsim 10^{-2}\,{\rm M}_\odot$. An estimate for the upper limit is not readily apparent in either system because we have no way of estimating the outer radius and, in particular, because the line-emitting gas could be only a thin outermost layer of the disc.

4 ROCHE LOBE OVERFLOW

In steady Roche lobe overflow accretion, the disc mass must be replenished on the viscous time-scale,

$$t_{\rm visc} = \frac{M_{\rm disc}}{\dot{M}}, \tag{13}$$

where the mass accretion rate $\dot{M} = L_{\rm x}/\eta c^2$ and η is an efficiency typically taken to be 0.1. We can also consider the viscous time-scale in a standard α-disc. We manipulate the familiar expression (Frank, King & Raine 2002), substituting azimuthal velocity for the radius via equation (7), and obtain

$$t_{\rm visc} \approx 4.2\alpha^{-4/5}\dot{M}_{16}^{-3/10} {M_1}^{3/2} {v_{100}}^{-5/2}\ {\rm yr}, \tag{14}$$

where $\dot{M}_{16}$ is the mass accretion rate in units 10^{16} g s^{-1}. For the X-ray luminosities given in Table 1, we find $\dot{M} \approx 2 \times 10^{19}$ g s^{-1} ($3 \times 10^{-7}\,{\rm M}_\odot\,{\rm yr}^{-1}$).

If we assume the 'edge-on' velocities discussed in relation to Fig. 3 and $\alpha = 0.1$, equations (13) and (14) require masses of 70 and 4000 M$_\odot$ for CXOJ033831.8−352604 and RZ2109, respectively. These numbers are surprisingly similar to the minimum masses

found in Section 2. The minimum masses are ∼40 times larger if the disc has $Z \approx 0.3\,Z_{\odot}$. The viscous time-scale $t_{\rm visc} \gtrsim 300$ yr.

Temperatures derived with the α-disc prescription, standard assumptions and the above limits are too cold by a factor of ∼10. M_1, $\dot{M}$ and α all enter as fairly weak powers and offer no obvious solution. Irradiation of a surface layer (e.g. Dubus et al. 1999) might yield the necessary temperatures.

Can a globular cluster form and sustain the massive accretion discs implied by the observed [O III] luminosities? Combining the minimum masses obtained in Section 2 with the rotational velocities derived above, we obtain $r_0 \approx 2 \times 10^{14}$ and 5×10^{14} cm, for CXOJ033831.8−352604 and RZ2109, respectively. We take this as the distance from the centre of the compact object to the Lagrange point L_1. We then assume a $1\,M_{\odot}$ donor star (giving mass ratios $q = 0.01$ and 1.7×10^{-4}) and employ approximations from Eggleton (1983) and Frank et al. (2002), and we obtain donor Roche lobe radii $r_{\rm L} \gtrsim 10^{13}$ and 5×10^{12} cm, respectively. These radii are comfortably within the size limits of the red giants that are common in globular clusters, but they represent lower limits. Larger central object masses would correspond to larger overflow radii (because the dependence of $r_{\rm L}/r_0$ on M via q is not enough to overcome $r_0 \propto M$). White dwarfs have been mentioned because of the apparent high metallicity in both systems. With prototypical $M_{\rm wd} = 0.6\,M_{\odot}$ and $r_{\rm wd} = 10^9$ cm, we can *strongly* exclude white dwarfs as Roche lobe overflow donors in either system.

Does the envelope of a red giant contain enough oxygen to produce the observed line luminosities? Carretta & Gratton (1997) considered the metallicities of red giants in 24 Galactic globular clusters. They found subsolar metallicities for every star in their study. The majority were subsolar by at least an order of magnitude. The most metal rich had $Z \approx 0.3\,Z_{\odot}$.

The [O III]/Hβ and [N II]/Hα values I10 observed in CXOJ033831.8−352604 ($\gtrsim$5 and $\gtrsim$7, respectively) and the [O III]/Hβ value Z08 observed in RZ2109 (∼30) are not necessarily indicative of high-metallicity gas. The photoionized gas near the centre of the giant H II region 30 Doradus has $Z \approx 0.3\,Z_{\odot}$ and [O III]/H$\beta \approx 6$ (Pellegrini et al. 2010). Elevated ratios are often thought to be signs of radiative shock heating (e.g. Dopita & Sutherland 1995), as was noted by Z08. Detailed attempts to distinguish between enhanced abundances and non-equilibrium heating processes are probably unwarranted without better observational constraints. A further complication pertains to whether the line-emitting gas is radiation or matter bound (McCall, Rybski & Shields 1985), although the high observed [N II]/Hα would seem to make the latter less likely in CXOJ033831.8−352604.

If Z08 are correct in their black hole wind explanation of RZ2109, we offer without comment the suggestion that the observed very broad linewidths may be the low-resolution appearance of narrow emission lines atop broader ones as in a two-wind structure (e.g. Fernandes 1999).

ACKNOWLEDGMENTS

RLP thanks referee John Raymond for excellent suggestions and criticisms and Joel Bregman, Gary Ferland, Jimmy Irwin, Jon Miller, Eric Pellegrini, Mark Reynolds and Pete Storey for fruitful discussions.

REFERENCES

Andreä J., Drechsel H., Starrfield S., 1994, A&A, 291, 869
Belczynski K. et al., 2010, ApJ, 714, 1217
Carretta E., Gratton R. G., 1997, A&AS, 121, 95
Dopita M. A., Sutherland R. S., 1995, ApJ, 455, 468
Dubus G., Lasota J.-P., Hameury J.-M., Charles P., 1999, MNRAS, 303, 139
Eggleton P., 1983, ApJ, 268, 368
Fabian A. C., Pringle J. E., Rees M. J., 1975, MNRAS, 172, 15
Ferland G. J. et al., 1998, PASP, 110, 761
Fernandes R. C. Jr, 1999, MNRAS, 305, 602
Frank J., King A., Raine D., 2002, Accretion Power in Astrophysics, 3rd edn. Cambridge Univ. Press, Cambridge
Grevesse N., Sauval A., 1998, Space Sci. Rev., 85, 161
Hui Y., Krolik J., 2008, ApJ, 679, 1405
Irwin J. A., Brink T. G., Bregman J. N., Roberts T. P., 2010, ApJ, 712, 1 (I10)
Kastner S. O., Bhatia A. K., 1989, ApJS, 71, 665
Keenan F. P., Aggarwal K. M., 1987, ApJ, 319, 403
King A. R., 2008, MNRAS, 385, 113
King A. R., 2009, MNRAS, 393, 41
McCall M. L., Rybski P. M., Shields G. A., 1985, ApJS, 57, 1
Miller J. M., Fabian A. C., Miller M. C., 2004, ApJ, 614, 117
Nussbaumer H., Storey P. J., 1981, A&A, 99, 177
Osterbrock D. E., Ferland G. J., 2006, in Osterbrock D. E., Ferland G. J. eds, Astrophysics of Gaseous Nebulae and Active Galactic Nuclei, 2nd edn. University Science Books, Sausalito, CA
Pellegrini E. et al., 2010, submitted
Ralchenko Yu., Kramida A. E., Reader J., NIST ASD Team (2008). NIST Atomic Spectra Database (version 3.1.5) (online), available at http://physics.nist.gov/asd3 (2010, March 29). National Institute of Standards and Technology, Gaithersburg, MD
Rosswog S., Ramirez-Ruiz E., Hix W. R., 2009, ApJ, 695, 404
Rybicki G. B., Lightman A., 1979, Radiative Processes in Astrophysics. Wiley, New York
Shakura N. I., Sunyaev R. A., 1973, A&A, 24, 337
Wiese W. L., Fuhr J. R., Deters T. M., 1996, J. Phys. Chem. Ref. Data, Monograph No. 7
Winter L. M., Mushotzky R. F., Reynolds C. S., 2006, ApJ, 649, 730
Zepf S. E. et al., 2007, ApJ, 669, 69
Zepf S. E. et al., 2008, ApJ, 683, 139 (Z08)

This paper has been typeset from a TEX/LATEX file prepared by the author.